Journal of Materials Chemistry A

Accepted Manuscript

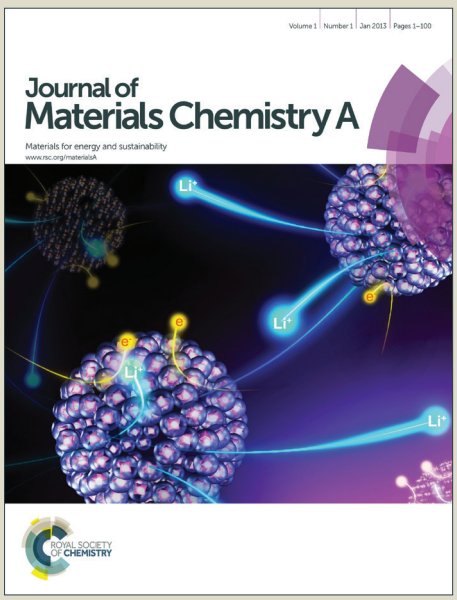

This is an *Accepted Manuscript*, which has been through the Royal Society of Chemistry peer review process and has been accepted for publication.

Accepted Manuscripts are published online shortly after acceptance, before technical editing, formatting and proof reading. Using this free service, authors can make their results available to the community, in citable form, before we publish the edited article. We will replace this *Accepted Manuscript* with the edited and formatted *Advance Article* as soon as it is available.

You can find more information about *Accepted Manuscripts* in the Information for Authors.

Please note that technical editing may introduce minor changes to the text and/or graphics, which may alter content. The journal's standard Terms & Conditions and the Ethical guidelines still apply. In no event shall the Royal Society of Chemistry be held responsible for any errors or omissions in this *Accepted Manuscript* or any consequences arising from the use of any information it contains.

ROYAL SOCIETY OF CHEMISTRY

www.rsc.org/materialsA

Journal of Materials Chemistry A

ARTICLE

Three-dimensional nickel hydroxide/graphene composite hydrogels and its transformation to NiO/graphene composites for energy storage

Xiaoqian Meng, Junwu Zhu*, Huiping Bi, Yongsheng Fu, Qiaofeng Han, Xin Wang

Received 00th January 20xx,
Accepted 00th January 20xx

DOI: 10.1039/x0xx00000x

www.rsc.org/

Graphene and its functionalized derivatives like graphene oxide (GO) have become handy and convenient building blocks for self-assembly to fabricate graphene-based functional materials with three-dimensional (3D) macroscopic structure. Herein, a convenient one-step hydrothermal method for preparing the $Ni(OH)_2$/graphene composite hydrogels (NGHs) with interconnected networks is described. This procedure contains the reduction of GO sheets by hydrazine and *in situ* deposition of $Ni(OH)_2$ nanoplates on graphene sheets. Notably, the obtained $NGH_{7.5}$ (the calculated mass ratio of formed $Ni(OH)_2$ with GO is 7.5:1) can offer a high specific capacitance of 1125.4 F g^{-1} at a charge/discharge rate of 0.5 A g^{-1}, which is almost 2.2 times and 8.1 times higher than $Ni(OH)_2$ and graphene, respectively. Meanwhile, the NGHs also present stable cycling performance with 87.3 % capacitance retention after 1000 cycles, which are significantly higher than that of its counterparts of $Ni(OH)_2$. More interestingly, the 3D structure of NGH can be easily transmitted to NiO/graphene (NiO/G) composites utilizing a facile thermal treatment procedure. The electrode based on NiO/G composite delivers a discharge capacity of 1349 mA h g^{-1} and a charge capacity of 992 mA h g^{-1} at the 1st cycle with a coulombic efficiency of about 73.5 %. This work opens a considerable way to fabricate functional graphene-based 3D structure and its composite materials, and makes a significant contribution to energy storage/conversion from alternative energy sources.

Introduction

The supercapacitors and lithium-ion batteries (LIB) have attracted extensive interest superior to traditional electric double-layer capacitors and batteries, and regarded as considerable candidates for energy storage.[1-8]

Recently, graphene has generated increasing attention for its potential applications in sensors, catalysis, energy-storage devices, environmental fields,[9-15] etc. However, suffering from the intersheet van der Waals attractions, the restacking of graphene sheets would inevitably occur in graphene assembling process, which seriously hinder them from practical applications.[16,17] Consequently, many excellent properties of graphene cannot be fully harnessed in its assembly.

Three-dimensional (3D) macroscopic graphene-based functional materials have been given extensive attention in recent years.[16-22] This unique 3D architecture can not only prevent excessive restacking of graphene sheets, but also offer free channels for ions diffusion. Especially, the graphene-based hydrogels and aerogels with 3D architecture reveal high surface areas, high conductivity, large specific capacitances, excellent rate capability and cycling stability, making them attractive electrode materials for supercapacitor.[19,23,24]

Thanks to the high theoretical capacitance and cost effectiveness, transition-metal oxides/hydroxides, such as NiO, $Ni(OH)_2$ and layered double hydroxides (LDHs) have been widely explored for electrode materials. Nevertheless, the capacitances of above materials severely compromised in bulk electrodes, because these materials are too insulating to support effective charge-transfer reactions. Moreover, due to the gradual loss of electroactive species during cycling process, their cycling performances are weaker compared to other electrode materials. Recent studies have demonstrated that the introduction of various carbon materials, such as active carbons, carbon nanotubes and graphene can greatly improve both the capacitance and cycling capability of NiO[5-8,25-27], $Ni(OH)_2$[28-36] and LDHs[38-41]. Actually, the $Ni(OH)_2$/graphene composites have been widely studied as electrode materials. For instance, Wang *et al*. demonstrated that the oxidation degrees of graphene sheets play an important role in the electrochemical performance and morphology of the obtained $Ni(OH)_2$/graphene nanomaterials.[2] Chen *et al*. fabricated a hybrid material composed of low defect density graphene-supported $Ni(OH)_2$ sheets *via* a soft chemistry route.[28] Moreover, the NiO/graphene transformed from $Ni(OH)_2$/rGO has also been studied in energy storage.[5-8,25-27,37] The obtained NiO/graphene composites were used as electrodes either for supercapacitors or lithium ion batteries. For example, Zhou *et al*. discussed the oxygen bridges between graphene and NiO, and the result verified that the oxygen bridges actually lead to the high-performance of NiO/graphene for lithium ion batteries.[6] Huang *et al.* demonstrated a facile general strategy to fabricate ultrathin porous NiO/graphene sheets, showing a

[a] *Key Laboratory for Soft Chemistry and Functional Materials (Nanjing University of Science and Technology), Ministry of Education, Nanjing 210094, China.*
**To whom correspondence should be addressed. E-mail: zhujw@njust.edu.cn*
Electronic Supplementary Information (ESI) available: [Additional data of obtained samples and electrochemical measurements with a two-electrode system]. See DOI: 10.1039/b000000x/

Journal of Materials Chemistry A Accepted Manuscript

remarkable lithium-storage performance than that of the bare NiO.[27] In addition, LDHs, known as hydrotalcite-like compounds or anionic clays, are a class of important lamellar materials. As a special type of metal hydroxides, LDHs are employed to prepare hybrid materials between graphene and LDHs, which can be directly used as electrodes for supercapacitors[38,39] or calcinated to obtain good composites for using in lithium ion batteries[40,41]. For example, Latorre-Sanchez *et al.* prepared GO/NiMn-LDH hybrid, which could lead to the deposition of Ni_6MnO_8 nanoparticles on larger reconstituted graphene sheets (G/NiMn) after calcination. The obtained G/NiMn was used as an anode for Li-ion batteries.[41]

Considering the multiple advantages of porous graphene hydrogels in comparison with other carbon materials, including enhanced transport property and mechanical flexibility, it is worthwhile to explore the possibility of combining $Ni(OH)_2$ and NiO with graphene into porous hydrogels to improve the electrochemical performance.[45]

Herein, we developed a convenient method for preparing 3D graphene hydrogels (GHs) and NGHs. Particularly, utilizing the gelation of graphene oxide enables the anchoring of $Ni(OH)_2$ nanoplates on surfaces of graphene sheets and the formation of 3D hydrogels to occur at the same time. Compared with GH and $Ni(OH)_2$, the electrochemical performance of NGHs is significantly improved. Specially, the 3D structure transmission from NGH bestows NiO/G an excellent electrochemical properties for lithium-ion batteries. This work highlights the beneficial synergistic effects between $Ni(OH)_2$, NiO and graphene-based hydrogels with unique 3D architecture.

Results and discussion

Formation of NGHs and their electrochemical properties for supercapacitors

In this process, when GO was reduced by hydrazine hydrate, at the same time, a small quantity of N atom could be introduced into this system from hydrazine hydrate. It has been reported that the heteroatoms and functional groups on graphene sheets may improve the wettability of electrode and enhance the overall capacitor performance owing to increased hydrophilic polar sites.[31]

Fig. 1a displays XRD patterns of the freeze-dried GO, GH, $Ni(OH)_2$ and $NGH_{7.5}$ samples. The XRD pattern of GO shows a large interlayer distance of 0.85 nm (2θ=10.3°) originated from the presence of hydroxyl, epoxy and carboxyl groups. In contrast to GO, after chemical reduction, the GH exhibits a relatively broadening signal around 25.3°, corresponding to a d-spacing of 0.35 nm. The broadening in peak width can be attributed to relatively disordered restacking of reduced GO sheets. As to $Ni(OH)_2$ and $NGH_{7.5}$, all diffraction peaks can be indexed to a single phase of well-crystallized hexagonal β-$Ni(OH)_2$ with the lattice parameters of a = b = 3.126 Å and c = 4.605 Å (JPCDS card No. 14-0117). It is noteworthy that, compared with GH, the diffraction peak of GO became nearly invisible in $NGH_{7.5}$, indicative of the high separation of graphene sheets caused by the combination of 3D structure and introduction of $Ni(OH)_2$ particles. In fact, with the aid of gelation of graphene oxide, the GO and its mixture with $Ni(OH)_2$ can produce the self-supported 3D hydrogels (Fig. 1d) through this hydrothermal procedure. Apparently, the NGHs present expansion to some content in volume in comparison with GH due to the intercalation of $Ni(OH)_2$ nanoparticles between graphene sheets. The unique 3D structure of NGHs can effectively prevent the restacking of graphene sheets, enabling both sides of graphene sheets and $Ni(OH)_2$ to expose to electrolyte, which is in favour of the improvement of electrochemical performance.

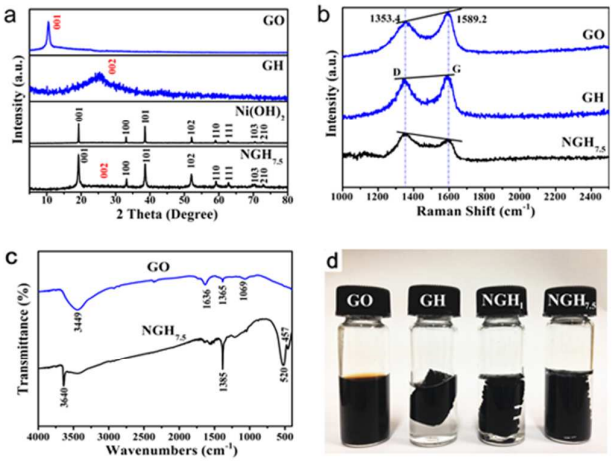

Fig. 1. (a) XRD patterns, (b) Raman spectra, and (c) FT-IR spectra of freeze-dried samples. (d) Photographs of GO dispersion, GH, NGH_1 and $NGH_{7.5}$.

To further examine the deoxygenation of GO, the obtained samples were subjected to Raman spectroscopy measurement. As shown in Fig. 1b, two prominent peaks of GO at 1353.4 and 1589.2 cm^{-1} are attributed to the D and G modes, respectively. Generally, the G mode is usually assigned to E_{2g} photon of sp^2 hybridized carbon, while the D mode is derived from a breathing mode of k-point photons of A_{1g} symmetry of disordered carbon. It is worth noting that the Raman spectra of GH and $NGH_{7.5}$ shows an increased D/G intensity ratio (0.95 and 1.20) compared to that of GO (0.84), suggesting the decrease in size of in-plane sp^2 domains and the presence of more disorder carbon framework in $NGH_{7.5}$. This result can be attributed to the declined restacking degree of graphene sheets because of the presence of $Ni(OH)_2$ particles, which matches very well with the XRD results.

The identity of functional groups incorporated in GO and $NGH_{7.5}$ were analyzed by FT-IR and XPS measurements. As shown in Fig. 1c, compared to GO, the weakening of characteristic peaks of oxygen-containing functional groups in $NGH_{7.5}$, including the stretching vibrations of -OH (H-O-H and C-OH) at around 3449 cm^{-1}, the stretching vibrations of carbon backbone at 1636 cm^{-1}, the O-H deformation vibrations of tertiary C-OH groups at 1365 cm^{-1}, and the C-O stretching vibrations of epoxy groups at 1069 cm^{-1}, indicates the

Journal of Materials Chemistry A Accepted Manuscript

This journal is © The Royal Society of Chemistry 20xx

reduction of GO caused by this hydrothermal process. Moreover, the narrow typical absorption located at around 3640 cm^{-1} in $NGH_{7.5}$ is due to the -OH groups in β-$Ni(OH)_2$. The absorption at 1385 cm^{-1} might originate from the interlayer nitrate anion.[32,43] Two peaks, which appear at 520 and 457 cm^{-1} in the low wavenumber region, correspond to the Ni-O-H stretching vibration and the Ni-O stretching mode, respectively.[14,28]

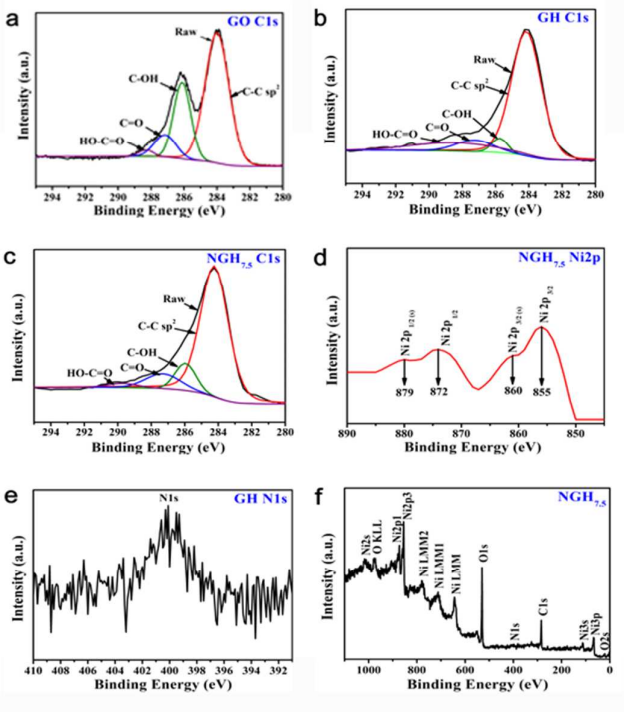

Fig. 2. XPS spectra of freeze-dried samples. (a) C1s spectrum of GO, (b, e) C1s and N1s spectra of GH, (c, d) C1s and Ni2p spectra of $NGH_{7.5}$, and (f) survey scan of $NGH_{7.5}$.

This conclusion is also supported by the XPS results. As shown in Fig. 2a, the C1s peak of GO can be deconvoluted into four components of C-C (284.0 eV), C-OH (286.1 eV), C-O-C (287.2 eV) and HO-C=O (288.3 eV), respectively. However, the intensities of these oxygen-containing groups in GH and $NGH_{7.5}$ are obviously weaker than those of GO (Fig. 2a-c), further indicating the occurrence of deoxygenation *via* this hydrothermal process. In addition, the Ni $2p_{3/2}$ peak is at 855.0 eV, and the Ni $2p_{1/2}$ peak locates at 872.0 eV, with a spin-energy separation of 17 eV (Fig. 2d). These results are in accordance with the reported data of Ni $2p_{3/2}$ and Ni $2p_{1/2}$ in $Ni(OH)_2$.[34] In addition, Fig. 2f reveals that the $NGH_{7.5}$ contains Ni, C, O and N as the main components. The presence of N1s shown in Fig. 2e and 2f further demonstrates the successful introduction of small quantity of N atom, which matches well with the previous discussion.

The morphology and microstructures of freeze-dried samples were characterized by TEM and SEM. Fig. 3d-f reveal that the $Ni(OH)_2$ is actually composed of nanoplates with a mean diameter of about 240 nm (see Supporting Information, Fig. S1), and few rod-liked particles shown in Fig. 3f seem like the standing nanoplates (see Supporting Information, Fig. S1). Nevertheless, GH and $NGH_{7.5}$ present a 3D porous morphology (Fig. 3a-c, g-i), in which the graphene sheets connect together with each other and form a porous network structure. Actually, with the aid of gelation of GO dispersion, the formation of 3D structured GH and NGHs can be attributed to the partial overlapping or coalescing of flexible reduced GO sheets *via* supramolecular interactions such as *π-π* stacking and hydrogen bonding.

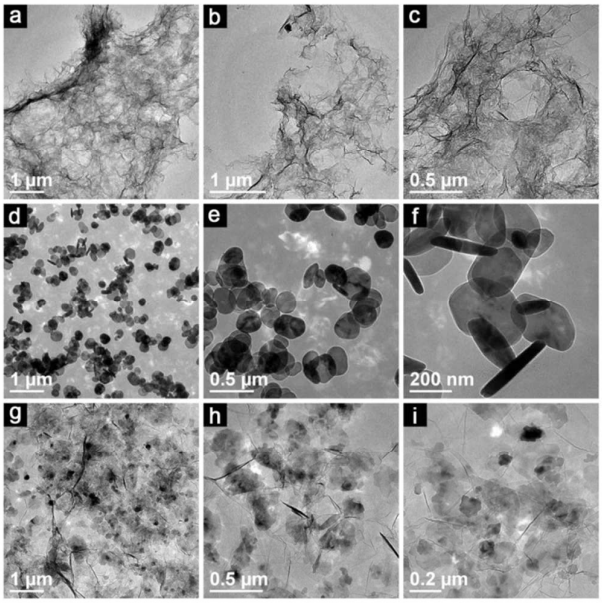

Fig. 3. TEM images of freeze-dried GH (a-c), $Ni(OH)_2$ (d-f), and $NGH_{7.5}$ (g-i).

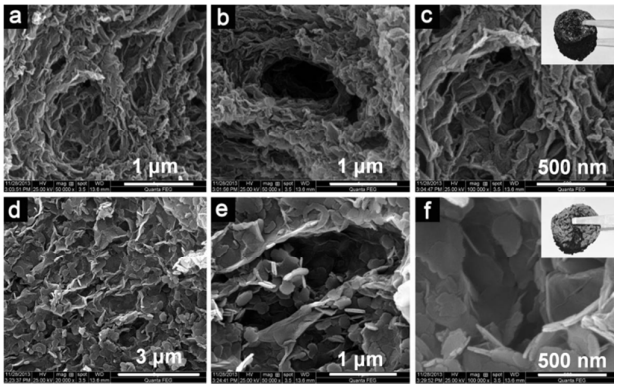

Fig. 4. SEM images of freeze-dried GH (a-c) and $NGH_{7.5}$ (d-f). The insets of (c) and (f) are photographs of freeze-dried GH and $NGH_{7.5}$.

The well-defined and interconnected 3D network of the resulting GH and NGHs were revealed by typical SEM images (Fig. 4). The TEM and SEM images of $NGH_{7.5}$ composite clearly demonstrate that $Ni(OH)_2$ nanoplates have anchored onto the surfaces of graphene sheets (Fig. 3g-i, Fig. 4d-f). Interestingly, there is a slight difference in sizes of $Ni(OH)_2$ between bare

Journal of Materials Chemistry A Accepted Manuscript

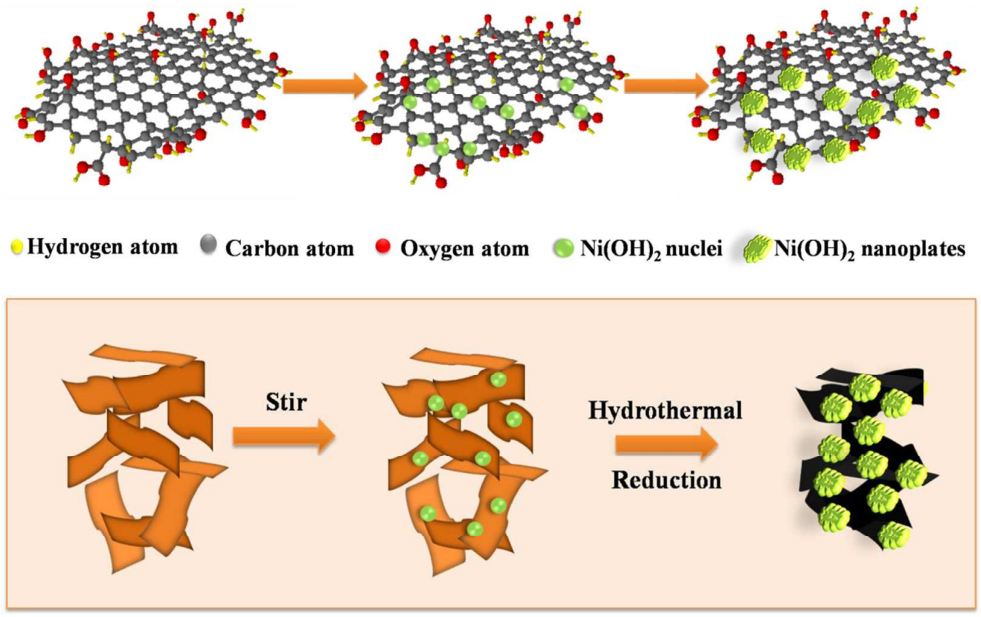

Fig. 5. Schematic illustration of the formation mechanism of NGHs

$Ni(OH)_2$ and $NGH_{7.5}$ composite. The $Ni(OH)_2$ nanoplates in $NGH_{7.5}$ behave smaller diameters than that of single $Ni(OH)_2$, suggesting a diverse crystals growth process on and out of GO supports. Furthermore, the presence of $Ni(OH)_2$ can effectively prevents the agglomeration or restacking of graphene sheets, which is favorable for increasing accessible reaction sites. The residual functional groups of graphene could provide preferred nucleation sites for the growth of $Ni(OH)_2$, thus enabling a good dispersion of $Ni(OH)_2$ on the graphene support. Consequently, all of these characterizations verify the successful anchoring of $Ni(OH)_2$ nanoplates onto graphene sheets and the chemical reduction of GO. Moreover, the typical freeze-dried hydrogels are sufficiently mechanically strong to allow handling with tweezers (insets of Fig. 4c, f).

The formation mechanism of NGHs is illustrated in Fig. 5. Generally, it is well known that the crystal growth process in an aqueous phase system consists of two stages: a nucleation stage and a growth stage. Firstly, the Ni^{2+} ions tended to adsorb onto surfaces of negative GO sheets *via* electrostatic interactions, which then would react with OH^- anions came from ammonia to produce numerous tiny *β*-$Ni(OH)_2$ nuclei. Afterwards, the formed crystals gradually grew into thin nanoplates and *in situ* deposited on both sides of graphene sheets. Meanwhile, be means of the gelation of graphene oxide, the reduced graphene oxide sheets anchored with $Ni(OH)_2$ nanoplates were simultaneously self-assembled into 3D hydrogels with interconnected networks driven by combined hydrophobic and *π*-*π* stacking interactions, due to the decrease of oxygenated groups on graphene sheets. Furthermore, the deposited $Ni(OH)_2$ nanoplates on graphene sheets facilitate the stabilization of such novel graphene hydrogels, which could serve as spaces to effectively inhibit the restacking of graphene sheets.

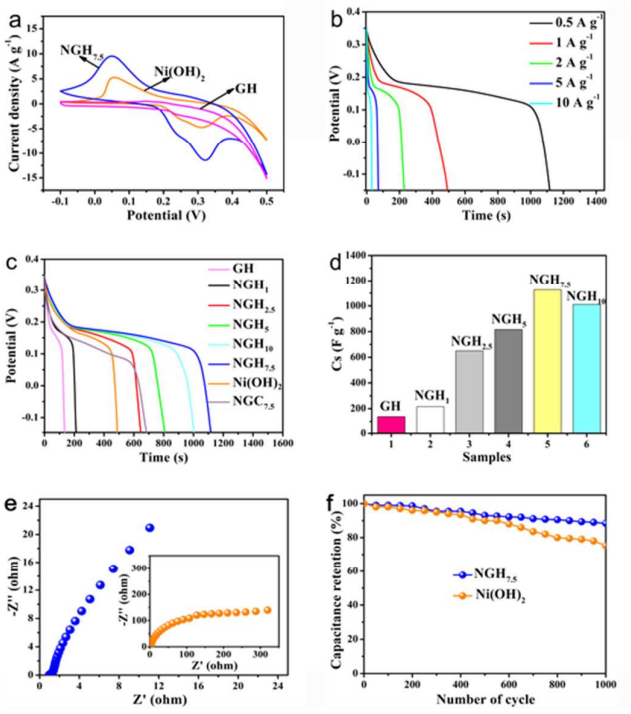

Fig. 6. (a) CV curves of freeze-dried GH, $Ni(OH)_2$ and $NGH_{7.5}$, (b) galvonostatic charge-discharge curves of freeze-dried $NGH_{7.5}$ at different current densities, (c) galvonostatic charge-discharge curves of different samples at a current density of 0.5 A g^{-1}, (d) Cs of freeze-dried NGHs with different ratios of $Ni(OH)_2$/GO, (e) Nyquist plots of freeze-dried $Ni(OH)_2$ and $NGH_{7.5}$, and (f) Cycle life of freeze-dried $Ni(OH)_2$ and $NGH_{7.5}$.

Journal of Materials Chemistry A Accepted Manuscript

This journal is © The Royal Society of Chemistry 20xx

Based on above discussion, we can see that the introducing of $Ni(OH)_2$ onto graphene sheets is an effective way for inhibiting the restacking of graphene sheets. Meanwhile, the presence of graphene sheets can effectively prevent $Ni(OH)_2$ nanoplates from aggregation. More importantly, the unique 3D structure endows NGHs with more active regions for depositing of $Ni(OH)_2$ nanoplates and more channels for the insertion/deinsertion of ions from electrolyte to electrode, leading to the improved electrochemical performance.

The as-obtained samples were fabricated into electrodes, and their electrochemical performances were characterized by Cyclic Voltammetry (CV), galvanostatic charge/discharge and electrochemical impedance spectroscopy (EIS) measurements using a three-electrode system (Fig. 6). Typical CV responses of freeze-dried GH, $Ni(OH)_2$ and $NGH_{7.5}$ at a scan rate of 5 mV s^{-1} are shown in Fig. 6a. The two voltammetric peaks observed in the CV plots of $Ni(OH)_2$ and $NGH_{7.5}$ are related to the following redox reactions: $Ni(OH)_2 + OH^- \leftrightarrow NiO(OH) + H_2O+e^-$. Obviously, the $NGH_{7.5}$ and $Ni(OH)_2$ present similar curve shape, implying that the capacitance of $NGH_{7.5}$ is mainly associated with the Faradaic pseudocapacitor.[28] Moreover, since *Cs* is proportional to the average areas of CVs, the results shown in Fig. 6a indicate that C_s increases from GH, $Ni(OH)_2$ to $NGH_{7.5}$. Apparently, the $NGH_{7.5}$ reveals a higher C_s in comparison with that of its components.

Galvanostatic charge/discharge measurements of $NGH_{7.5}$ at different current densities were conducted and shown in Fig. 6b. The *Cs* value is calculated according to $Cs=I/[m(dV/dt)]$, where *I* is the constant discharge current, *m* is the mass of active electrode material, and dV/dt can be obtained from the discharge curve. It is impressive that the $NGH_{7.5}$ has high C_s of 1125.4, 996.6, 937.7, 759.0 and 695.0 F g^{-1} at discharge current densities of 0.5, 1, 2, 5 and 10 A g^{-1}, respectively. Significantly, about 61.8 % of initial C_s could be retained when the current density increased from 0.5 to 10 A g^{-1}, indicating a good rate capability.

Furthermore, the ratios of $Ni(OH)_2$/GO have a great influence on its electrochemical properties. As shown in Fig. 6c and d, the C_s increases with the elevated ratios of $Ni(OH)_2$/GO from 1 to 7.5. However, the C_s declines when the ratio further increases to 10. In fact, with the gradual increase of $Ni(OH)_2$/GO ratios, too many $Ni(OH)_2$ nanoparticles around graphene sheets induce their aggregation, leading to poor dispersion of $Ni(OH)_2$ nanoparticles on graphene sheets. Some $Ni(OH)_2$ nanoparticles deposited on graphene sheets would inevitably aggregate, accompanied by the decrease of conductivity; meanwhile, some $Ni(OH)_2$ nanoparticles might even scatter out of the graphene supports if the $Ni(OH)_2$/GO ratios continue to increase, and the independent 3D nanostructure of hydrogels would be destroyed. It would have a negative influence on synergistic effect between $Ni(OH)_2$ and graphene, resulting in the decrease of C_s. As depicted in Fig. 6c, the calculated C_s values of GH, $Ni(OH)_2$, $NGC_{7.5}$ ($Ni(OH)_2$/graphene composite) and $NGH_{7.5}$ are 137.8, 496.5, 730.3 and 1125.4 F g^{-1}, respectively. Obviously, the $NGH_{7.5}$ exhibits significantly higher C_s value than that of its counterparts, indicative of the distinctive synergistic effect between $Ni(OH)_2$ and GHs, corresponding to the CV results. In particular, the $NGC_{7.5}$ shows a medial C_s between $Ni(OH)_2$ and $NGH_{7.5}$ (Fig. 6c and Fig. S2a). In contrast to $NGC_{7.5}$, the more superior performance presented by $NGH_{7.5}$ can be ascribed to the formation of highly open and porous framework, which is originated from the hydrogels.

EIS analysis is a principle method to examine the fundamental behavior of electrode materials for supercapacitors. As can be seen from Fig. 6e, all Nyquist plots were characterized by two distinct parts: an inconspicuous arc in the high-frequency region and a linear line in the low-frequency region. Obviously, compared with $NGH_{7.5}$, the diffusive line of $Ni(OH)_2$ at lower frequency region comes away from an ideally straight line, suggesting the increasing diffusion resistance of ions and increased intrinsic resistance of charge transfer due to faradic reactions. Meanwhile, the graphene sheets overlap each other to form a conductive 3D network through sheet plane contact, which facilitates fast electron transfer between the active materials and the charge collector, resulting in the improvement of electrochemical performance of NGHs. This result is in good agreement with the capacitance values calculated from the CV curves and charge/discharge curves. Furthermore, the electrochemical stability of $Ni(OH)_2$ and $NGH_{7.5}$ was investigated at 0.5 A g^{-1} and shown in Fig. 6f. It is found that the $NGH_{7.5}$ electrode retains about 87.3 % of initial capacitance after 1000 cycles, better than that of the $Ni(OH)_2$ electrode with about 75.3 % maintenance. Notably, compared to its individual components, the enhanced electrochemical performances of as-obtained NGHs can be ascribed to the synergic effects of $Ni(OH)_2$ and graphene sheets or their integrated properties, making NGHs an optional and attractive electrode material for supercapacitor applications.

In addition, we have conducted the Ragone measurements through a two-electrode system (see Supporting Information, Fig. S2b). The energy density and maximum power density were calculated based on the mass of electrode materials in single electrode (see Supporting Information, SI-2). Seen from the result, $NGH_{7.5}$ can offer an energy density of 11.1 Wh kg^{-1} and maximum power density of 165.2 kW kg^{-1}, respectively. Both the energy density and maximum power density of $NGH_{7.5}$ are significantly higher than those of $Ni(OH)_2$, which only delivers an energy density of 3.6 Wh kg^{-1} and a maximum power density of 55.3 kW kg^{-1}, respectively. These results further demonstrate the more superior performances of $NGH_{7.5}$ than that of $Ni(OH)_2$.

Transformation of NGHs to NiO/G and the electrochemical properties for Li-ion batteries

As described at the experimental section, the heat treatment of $Ni(OH)_2$ and $NGH_{7.5}$ at 300 ^oC in N_2 for 2 h can lead to the formation of NiO and NiO/G composite. As shown in Fig. 7a, all the diffraction peaks can be indexed to the face-centered cubic (fcc) NiO phase (a=0.41780 nm, JCPDS file No. 71-1179).[44] No peaks assigned to β-$Ni(OH)_2$ can be observed in NiO and NiO/G, indicating that β-$Ni(OH)_2$ is completely converted to NiO after

Journal of Materials Chemistry A Accepted Manuscript

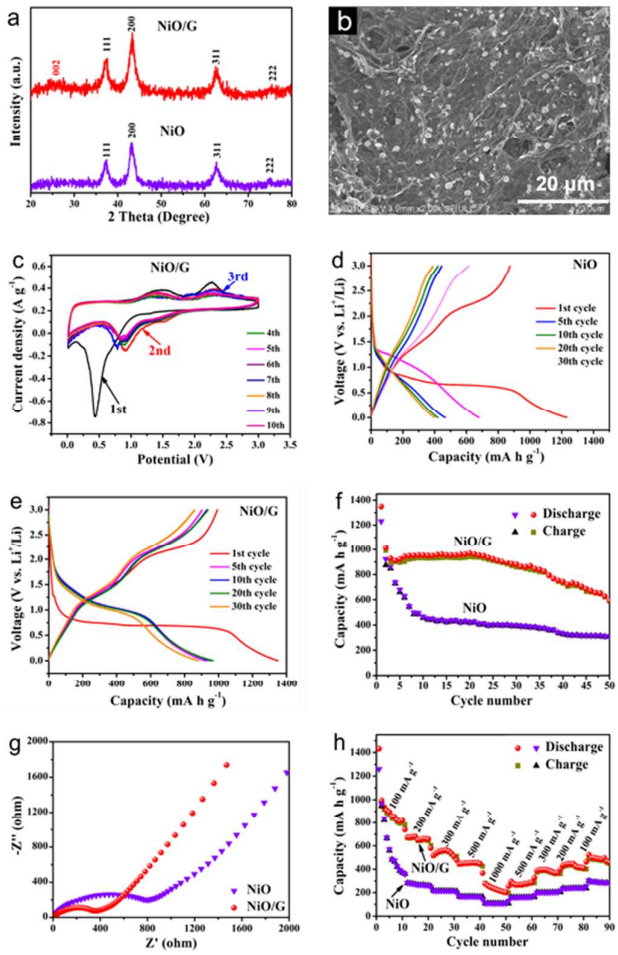

Fig. 7. (a) XRD patterns of NiO and NiO/G, (b) SEM image of NiO/G, (c) CV curves of NiO/G at a scan rate of 0.1 mV s^{-1} from 0.01 to 3 V, (d, e) galvanostatic charge discharge profiles of NiO and NiO/G at a current density of 50 mA g^{-1} for 50 cycles, (f) cycling performance of NiO and NiO/G, (g) Nyquist plots of NiO and NiO/G as anode materials measured after CV curves, (h) rate performance of NiO and NiO/G at different current densities.

being heated at 300 °C. Meanwhile, the FT-IR and Raman spectra of NiO and NiO/G were further demonstrated the successful preparation of NiO and NiO/G (see Supporting Information, Fig. S3), which is in accord with reported results.[6, 37, 45] The morphology of NiO and NiO/G was characterized by SEM (Fig. S3, Fig. 7b), revealing that NiO/G is actually composed of nanoplate-like NiO with average diameters of 500 nm anchored on graphene sheets, and the NiO nanoplates were evolved from $Ni(OH)_2$ nanoplates. While the SEM images of pure NiO (Fig. S3c-f) show that the sample consists of aggregated nanoplates with diameters of 200-500 nm. Significantly, as shown in Fig. S3g-i, the 3D structure of NGH was successfully transmitted to NiO/G through the thermal treatment procedure.

Fig. 7c shows the first ten CV curves of NiO/G at a scan rate of 0.1 mV s^{-1} from 0.01 to 3 V. It can be seen that the first cycle is obviously different from the second one. It also shows two cathodic peaks at about 0.7 and 0.4 V during the first cycle, corresponding to the electrochemical reduction reaction of NiO according to 2Li + NiO → Li_2O + Ni and solid electrolyte interface film.[7] The cathodic peaks shift to about 1.4 and 0.9 V, respectively, and become smaller since the 2nd cycle. The anodic peaks at 1.5 and 2.0 V shown in the charge cycles correspond to an oxidation reaction of NiO, in which NiO is formed from the reaction between Ni and Li_2O. The integral area and peak intensity in the following cycles are close to that of the 2nd cycle, indicating that the electrochemical cycle of NiO/G based electrode tends to stable after the 2nd cycle.

Galvanostatic charge-discharge experiments were carried out to evaluate the electrochemical performances of NiO/G composite. For comparison, the electrodes made of NiO were also tested under the same electrochemical conditions. The 1st, 5th, 10th, 20th and 30th charge-discharge curves of NiO and NiO/G under a current density of 50 mA g^{-1} are presented in Fig. 7d-e, respectively. As shown in Fig. 7e, the electrode based on NiO/G composite delivers a discharge capacity of 1349 mA h g^{-1} and a charge capacity of 992 mA h g^{-1} at the 1st cycle with a coulombic efficiency of about 73.5 %. Furthermore, NiO/G composite still shows a high reversible capacity of 881 mA h g^{-1} after 30 discharge-charge cycles (Fig. 7e). In contrast, the electrode based on NiO has a capacity of 1232 mA h g^{-1} in the first discharge step and a reversible capacity of 874 mA h g^{-1} in the initial charge step (Fig. 7d). However, it suffers from a fast fading of reversible capacity since the following cycles. Fig. 7f shows the cyclic performances of NiO and NiO/G at a current density of 50 mA g^{-1}. After 50 charge-discharge cycles, NiO/G still maintains a capacity of 592 mA h g^{-1}, while NiO only offers a low capacity of 311 mA h g^{-1}.

The combination of graphene with NiO also endows the NiO/G composite with good conductivity, which can be confirmed by the EIS measurements. The Nyquist plots after ten CV cycles were shown in Fig. 7g, in which the plot is constituted by a single depressed semicircles in the high-medium frequency region and an inclined line at low frequency, which can be assigned to the surface film resistance, charge transfer impedance, respectively [26]. Obviously, the diameter of the second semicircle for NiO/G is smaller than that of NiO, revealing lower charge transfer impedance. This phenomenon indicates that the electronic conductivity of NiO is improved after the incorporation of graphene, which would enable NiO/G composite with high electrical conductivity, rapid charge-transfer process, and good Li-ion kinetics for lithium uptake and extraction. Therefore, the NiO/G exhibits better rate performance compared to NiO, as shown in Fig. 7h. The reversible capacity of NiO/G is stable at ca. 800 mA h g^{-1} after 10 cycles at a current density of 100 mA g^{-1}. Upon increasing current density to 500 and 1000 mA g^{-1}, its reversible capacities are still maintained at ca. 442 and 202 mA h g^{-1}, corresponding to 46.7 % and 21.3 % capacity retention of the first capacity, respectively. When the current density returns to the initial 100 mA g^{-1} after 90 cycles, NiO/G composite recovers 47.3 % of its first capacity, indicating the relatively stable structure of the electrode. These performances are remarkably superior to that of pure NiO. For example, when the current density is 1000 mA g^{-1} and returns

Journal of Materials Chemistry A Accepted Manuscript

This journal is © The Royal Society of Chemistry 20xx

to the initial 100 mA g^{-1} after 90 cycles, the reversible capacity of pure NiO only delivers 109 and 284 mA h g^{-1} corresponding to only 11.5 % and 30 % capacity retention of the first capacity. The attractive electrochemical performance exhibited by NiO/G could be attributed to the directly grown of NiO nanoplates on graphene sheets, including a synergistic effect from the two components. Notably, NiO/G composite in our experiment was transformed from $Ni(OH)_2$/graphene hydrogels (NGHs). Interestingly, both the nanoplate-liked $Ni(OH)_2$ and the 3D framework of NGH was well inherited by NiO/G after calcination. The unique nanostructure of NiO/G effectively prevents the restacking of graphene sheets, and keeps good adhesion and electrical contact between NiO and graphene sheets. Therefore, the improved capacity value and cycling performance of NiO/G could be ascribed to the inheritance of the excellent properties of graphene hydrogels system.

Conclusions

In conclusion, we have successfully prepared NGHs with porous network structure *via* a one-step hydrothermal method to act as an advanced electrochemical material for supercapacitors. In NGHs, the $Ni(OH)_2$ nanoplates are uniformly grown on graphene sheets *in situ* while the graphene sheets self-assemble into a 3D porous framework. The unique hierarchical structure endows it with high specific capacitance and long cycle life for electrode materials. In addition, NiO/G composite transformed from NGHs shows highly reversible capacities and good rate capabilities for lithium ion batteries. Therefore, our study opens a new way to the design and fabrication of functional 3D hydrogels, and provides a new train of thought on electrode materials for energy storage.

Experimental section

Preparation and Purification of GHs and NGHs

As the raw materials, GO was prepared from natural powdered flake graphite (400 mesh) through a modified Hummers' method.[24] A typical route for the synthesis of NGH composite, when the calculated mass ratio of formed $Ni(OH)_2$ with feeding GO is 7.5:1, is as follows. In brief, 150 μL of hydrazine and 4 mL of $Ni(NO_3)_2$ solution (0.82 g of $Ni(NO_3)_2{\cdot}6H_2O$ dissolved in 4 mL of deionized water) were quickly poured into 10 mL of GO dispersion (3.5 mg mL^{-1}). After vigorous stirring for 0.5 h, 220 μL of $NH_3{\cdot}H_2O$ was added into the above mixture to form a homogeneous suspension. Afterwards, copies of 2.5 mL suspension were packed into several glass bottles, which were loaded into a Teflon-lined stainless steel autoclave and heated at 180 ^{o}C for 5 h. In order to keep enough vapor pressure, some quantity of deionized water was injected around the bottles. After cooling to room temperature, the obtained NGHs were carefully taken out, immersed into water and purified by dialysis overnight to remove the residual ions. The obtained hydrogel is defined as $NGH_{7.5}$. Analogously, the hydrogels with different mass ratios of $Ni(OH)_2$/GO, were labeled as NGH_{ratio} (e.g. NGH_1, $NGH_{2.5}$, NGH_5 and NGH_{10}).

For comparison, the pure GHs were prepared by using the same experimental procedure, but in the absence of $Ni(OH)_2$. Another control sample of bare $Ni(OH)_2$ was also obtained without GO.

To demonstrate the superiority of 3D architecture, instead of the hydrothermal treatment for NGH, the same precursor solution of $NGH_{7.5}$ was directly heated at 100 ^{o}C for 5 h in an oil bath with vigorous stirring to produce the $Ni(OH)_2$/graphene composite ($NGC_{7.5}$).

The samples, including $Ni(OH)_2$ and $NGH_{7.5}$, were heated to 300 ^{o}C with a ramp of 1 ^{o}C min^{-1} for 2 h under an nitrogen atmosphere to achieve their transmission for the formation of NiO and NiO/G.

Structure characterization

Powder X-ray diffraction (XRD) analyses were performed on a Bruker D8 Advance diffractometer with Cu Kα radiation (λ = 1.5418 Å). Raman spectroscopy was recorded with a Renishaw Raman microscope. Fourier transform infrared spectroscopy (FTIR) spectra of KBr powder pressed pellets were recorded on a FTIR-8400S spectrometer. Morphologies of as-obtained products were observed on a transmission electron microscope (TEM, JEOL JEM-2100) and scanning electron microscope (SEM, JEOL JSM-7001F). X-ray photoelectron spectra (XPS) were recorded on a PHI QUANTERA II X-ray photoelectron spectrometer, using monochromatic Al Kα radiation as the exciting source (energy resolution < 0.60 eV).

Electrochemical characterization of electrode materials for supercapacitors

The electrochemical properties of as-obtained products were investigated on a CHI760D electrochemical workstation (Shanghai CH Instrument company). The working electrodes were fabricated by mixing the freeze-dried samples with 15 wt% of acetylene black and 5 wt% of polytetrafluoroethylene (PTFE) binder. A small amount of deionized water was added to the mixture to produce a homogeneous paste. The mixture was coated on Ni foam to make electrodes and dried at 60 ^{o}C for 12 h. Before the electrochemical test, the prepared electrode was soaked in a 6 M of KOH solution overnight. Electrochemical characterizations were carried out in a conventional three-electrode cell with 6 M of KOH aqueous solution as the electrolyte. Platinum foil and a saturated calomel electrode (SCE) were used as the counter and reference electrodes, respectively. The details for the preparation process of electrodes using a two-electrode system were provided in the SI-2 (Supporting Information).

Electrochemical characterization of electrode materials for Li-ion batteries

The electrochemical properties of NiO and NiO/G as anode materials in half cells were evaluated by a galvanostatic charge/discharge technique. The test electrodes were prepared by mixing 80 wt% of active material, 10 wt% of acetylene black, and 10 wt% of the binder (poly(vinylidene

Journal of Materials Chemistry A Accepted Manuscript

Please do not adjust margins

difluoride), PVDF) dissolved in N-methyl pyrrolidinone to form a slurry, which was then coated onto a copper foil and dried under vacuum at 120 ^{o}C for 12 h. Half cells using Li foil as counter and reference electrode were assembled with Lab-made Swagelok cells for electrochemical measurement. The electrolyte was 1 M $LiPF_6$ in a 1: 1 v/v mixture of ethylene carbonate (EC) and diethyl carbonate (DEC). A Celgard 2400 porous membrane was used as the separator. The charge-discharge performances of the fabricated cells were tested between 0 and 3 V *vs.* Li^+/Li using a battery test system (LAND CT2001A). Cyclic voltammetry (CV) was conducted on a CHI760D electrochemical workstation at a scan rate of 0.1 mV s^{-1}.

Acknowledgements

This investigation was supported by the Jiangsu Funds for Distinguished Young Scientists (BK2012035), Program for New Century Excellent Talents in University (NCET-11-0834), the Natural Science Foundation of China (No. 51322212, 51472122), the Fundamental Research Funds for the Central Universities (No. 30920130111004) and PAPD of Jiangsu.

Notes and references

1 Y. Xu, Q. Wu, Y. Sun, H. Bai and G. Shi, *ACS Nano*, 2010, **4**, 7358-7362.
2 H. Wang, H. S. Casalongue, Y. Liang and H. Dai, *J. Am. Chem. Soc.*, 2010, **132**, 7472-7477.
3 M. Winter and R. J. Brodd, *Chem. Rev.*, 2004, **104**, 4245-4270.
4 P. Simon and Y. Gogotsi, *Nat. Mater.*, 2008, **7**, 845-854.
5 L. Tao, J. Zai, K. Wang, Y. Wan, H. Zhang, C. Yu, Y. Xiao and X. Qian, *RSC Adv.*, 2012, **2**, 3410.
6 G. Zhou, D. Wang, L.Yin, N. Li, F. Li and H. Cheng, *ACS Nano*, 2012, **6**, 3214-3223.
7 S. Hwang, G. K. Kim, SYun and K. Ryu, *Electrochim. Acta*, 2012, **78**, 406-411.
8 I. R. Kottegoda, N. H. Idris, L. Lu, J. Wang and H.-K. Liu, *Electrochim. Acta*, 2011, **56**, 5815-5822.
9 F. Schedin, A. Geim, S. Morozov, E. Hill, P. Blake, M. Katsnelson and K. Novoselov, *Nat. Mater.*, 2007, **6**, 652-655.
10 Y. Li, H. Wang, L. Xie, Y. Liang, G. Hong and H. Dai, *J. Am. Chem. Soc.*, 2011, **133**, 7296-7299.
11 S. Yin, Y. Zhang, J. Kong, C. Zou, C. M. Li, X. Lu, J. Ma, F. Y. C. Boey and X. Chen, *ACS Nano*, 2011, **5**, 3831-3838.
12 V. Chandra, J. Park, Y. Chun, J. W. Lee, I. Hwang and K. S. Kim, *ACS Nano*, 2010, **4**, 3979-3986.
13 C. Wang, J. Zhu, S. Liang, H. Bi, Q. Han, X. Liu and X. Wang, *J. Mater. Chem. A*, 2014, **2**, 18635-18643.
14 H. Wang, J. Gao, Z. Li, Y. Ge, K. Kan and K. Shi, *CrystEngComm*, 2012, **14**, 6843-6852.
15 Z. Zhang, J. Zhu, Q. Han, H. Cui, H. Bi and X. Wang, *Appl. Surf. Sci.,* 2014, **321**, 404-411.
16 Y. Xu, X. Huang, Z. Lin, X. Zhong, Y. Huang and X. Duan, *Nano. Res.*, 2013, **6**, 65-76.
17 X. Yang, J. Zhu, L. Qiu and D. Li, Adv. Mater., 2011, **23**, 2833-2838.
18 H. Gao, Y. Sun, J. Zhou, R. Xu and H. Duan, *ACS Appl. Mater. Inter.*, 2013, **5**, 425-432.
19 B. Adhikari, A. Biswas and A. Banerjee, *ACS Appl. Mater. Inter.*, 2012, **4**, 5472-5482.
20 B. Adhikari, A. Biswas and A. Banerjee, *Langmuir*, 2011, **28**, 1460-1469.
21 .Q. Y. Cheng, D. Zhou, Y. Gao, Q. Chen, Z. Zhang and B. Han, *Langmuir*, 2012, **28**, 3005-3010.
22 H. Bi, X. Xie, K. Yin, Y. Zhou, S. Wan, L. He, F. Xu, F. Banhart, L. Sun and R. S. Ruoff, *Adv. Funct. Mater.*, 2012, **22**, 4421-4425.
23 J. Yuan, J. Zhu, H. Bi, X. Meng, S. Liang, L. Zhang and X. Wang, *Phys. Chem. Chem. Phys.*, 2013, **15**, 12940-12945.
24 J. Yuan, J. Zhu, H. Bi, Z. Zhang, S. Chen, S. Liang and X. Wang, *RSC Adv.*, 2013, **3**, 4400-4407.
25 Y. Zou and Y. Wang, *Nanoscale*, 2011, **3**, 2615-2620.
26 Y. Mai, S. Shi, D. Zhang, Y. Lu, C. Gu and J. Tu, *J. Power Sources*, 2012, **204**, 155-161.
27 Y. Huang, X. Huang, J. Lian, D. Xu, L. Wang and X. Zhang, *J. Mater. Chem.*, 2012, **22**, 2844-2847.
28 J. Zhu, S. Chen, H. Zhou and X. Wang, *Nano. Res.*, 2012, **5**, 11-19.
29 Y. Wang, Z. Shi, Y. Huang, Y. Ma, C. Wang, M. Chen and Y. Chen, *J. Phys. Chem. C*, 2009, **113**, 13103-13107.
30 L. Zhang and G. Shi, *J. Phys. Chem. C*, 2011, **115**, 17206-17212.
31 S. Stankovich, D. A. Dikin, R. D. Piner, K. A. Kohlhaas, A. Kleinhammes, Y. Jia, Y. Wu, S. T. Nguyen and R. S. Ruoff, *Carbon*, 2007, **45**, 1558-1565.
32 J. Yan, Z. Fan, W. Sun, G. Ning, T. Wei, Q. Zhang, R. Zhang, L. Zhi and F. Wei, *Adv. Funct. Mater.*, 2012, **22**, 2632-2641.
33 J. W. Lee, T. Ahn, D. Soundararajan, J. M. Ko and J.-D. Kim, *Chem. Commun.*, 2011, **47**, 6305-6307.
34 S. Yang, X. Wu, C. Chen, H. Dong, W. Hu and X. Wang, *Chem. Commun.*, 2012, **48**, 2773-2775.
35 Y. Zhang, F. Xu, Y. Sun, Y. Shi, Z. Wen and Z. Li, *J. Mater. Chem.*, 2011, **21**, 16949-16954.
36 S. Chen, J. Duan, M. Jaroniec and S. Z. Qiao, *J. Mater. Chem. A*, 2013, **1**, 9409-9413.
37 B. Zhao, J. Song, P. Liu, W. Xu, T. Fang, Z. Jiao, H. Zhang and Y. Jiang, *J. Mater. Chem.*, 2011, **21**, 18792-18798.
38 Z. Gao, J. Wang, Z. Li, W. Yang, B. Wang, M. Hou, Y. He, Q. Liu, T. Mann, P. Yang, M. Zhang and L. Liu, *Chem. Mater.*, 2011, **23**, 3509-3516.
39 Y. Wimalasiri, R. Fan, X. S. Zhao and L. Zou, *Electrochim. Acta*, 2014, **134**, 127-135.
40 D. Du, W. Yue, Y. Ren and X. Yang, *J. Mater. Sci.*, 2014, **49**, 8031-8039.
41 M. Latorre-Sanchez, P. Atienzar, G. Abellán, M. Puche, V. Fornés, A. Ribera and H. García, *Carbon*, 2012, **50**, 518-525.
42 S. Chen, J. Duan, Y. Tang and S. Z. Qiao, *Chem-Eur. J.*, 2013, **19**, 7118-7124.
43 L. Xu, Y.-S. Ding, C.-H. Chen, L. Zhao, C. Rimkus, R. Joesten and S. L. Suib, *Chem. Mater.*, 2007, **20**, 308-316.
44 Y. Wang, Q. Zhu and H. Zhang, *Chem. Commun.*, 2005, 5231-5233.
45 X. Xia, J. Tu, J. Zhang, X. Wang, W. Zhang and H. Huang, *Solar Energy Mater. Solar Cells*, 2008, **92**, 628-633.

Journal of Materials Chemistry A Accepted Manuscript

This journal is © The Royal Society of Chemistry 20xx

Three-dimensional nickel hydroxide/graphene composite hydrogels and its transformation to NiO/graphene composites for energy storage

Xiaoqian Meng, Junwu Zhu*, Huiping Bi, Yongsheng Fu, Qiaofeng Han, Xin Wang

Graphical Abstract

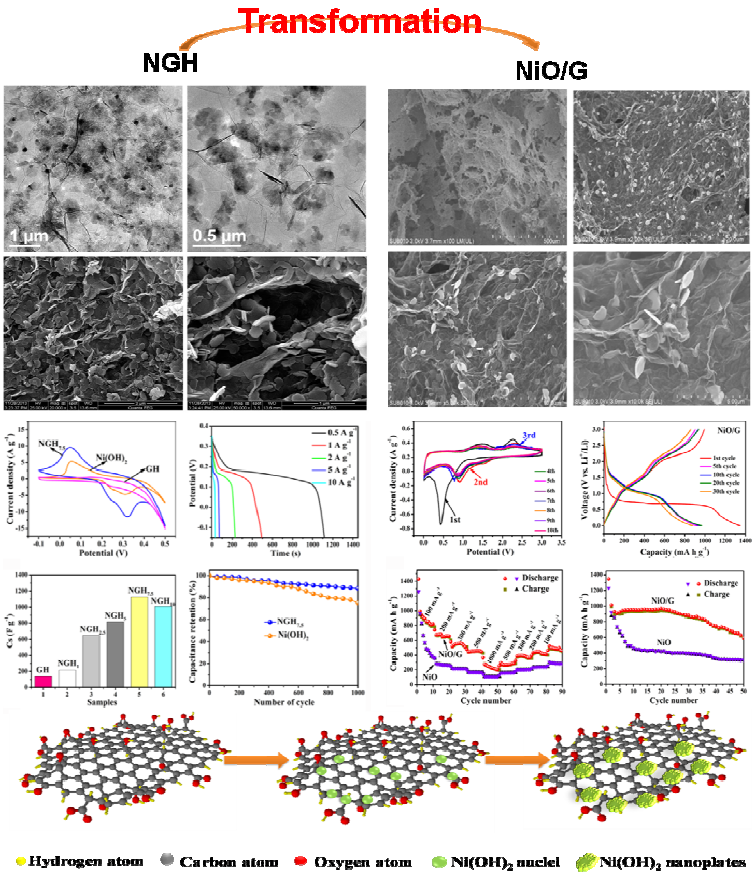

The $Ni(OH)_2$/graphene composite hydrogels are successfully prepared, in which the $Ni(OH)_2$ nanoplates are uniformly grown on graphene sheets *in situ* while the graphene sheets self-assemble into a 3D porous framework. The unique structure endows more channels for the insertion/deinsertion of ions from electrolyte to electrode, leading to the improved electrochemical performance. More interestingly, NGHs can be easily transmitted to NiO/graphene (NiO/G) composites utilizing a facile thermal treatment procedure. And the NiO/G composite transformed from NGH maintains the 3D structure and shows highly reversible capacities and good rate capabilities for lithium ion batteries.

Journal of Materials Chemistry A Accepted Manuscript